Chemical Engineering Journal 346 (2018) 57–64

Contents lists available at ScienceDirect

Chemical Engineering Journal

journal homepage: www.elsevier.com/locate/cej

Constructing fast electron and ion conductive framework for Li_2S as advanced lithium sulfur battery

Yueying Peng[a], Yiyong Zhang[a], Zhipeng Wen[a], Yunhui Wang[a], Zhiqiang Chen[a], Bing-Joe Hwang[b], Jinbao Zhao[a,*]

[a] *State Key Lab of Physical Chemistry of Solid Surfaces, Collaborative Innovation Centre of Chemistry for Energy Materials, State-Province Joint Engineering Laboratory of Power Source Technology for New Energy Vehicle, College of Chemistry and Chemical Engineering, Xiamen University, Xiamen 361005, PR China*

[b] *NanoElectrochemistry Laboratory, Department of Chemical Engineering, National Taiwan University of Science and Technology, Taipei 106, Taiwan*

HIGHLIGHTS

- Hollow Li_2S/CNT/C-N/O composite is obtained by Spray-dried technology.
- The interwoven CNT/C structure can provide great electron and Li-ion pathway.
- Great cycling stability and rate performances can be achieved.

GRAPHICAL ABSTRACT

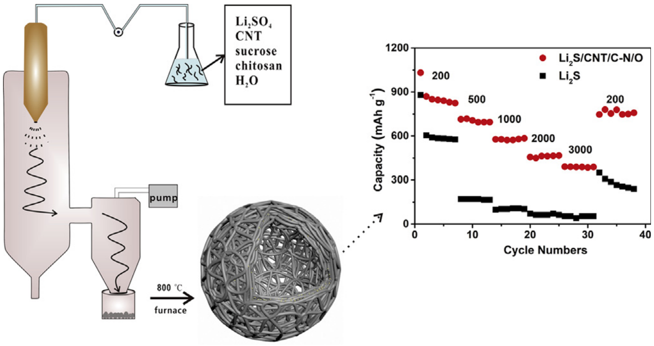

ARTICLE INFO

Keywords:
Lithium sulfur battery
Lithium sulfide cathode
Spray-dried technology
Electron and ion conductivity
In-situ electrochemical impedance spectra

ABSTRACT

Lithium sulfide (Li_2S) cathode is considered as a prospective substitution for sulfur-based cathode for as its high specific capacity. Despite this, the poor electron and lithium ion transportation for Li_2S impedes its further development. Herein, a great electron and lithium ion pathway is constructed for Li_2S by a facile spray-dried technology. In this composite, the nano-sized Li_2S is well imbedded in framework composed by the nitrogen/oxygen dual doped carbon nanotube/carbon (Li_2S/CNT/C-N/O). The electrochemical tests show that the prepared Li_2S/CNT/C-N/O cathode exhibits great cycling stability and rate capacity. A high initial discharge capacity of 1014 mAh g^{-1} is achieved with 671 mAh g^{-1} capacity remained at 200 mA g^{-1} after 200 cycles. Impressively, a stable capability is still exhibited from 200 to 3000 mA g^{-1} during rate testing. *In-situ* electrochemical impedance spectra test is further used to get insightful understanding about the improvements. The result reveals that decreased resistance and increased lithium-ion diffusion can be achieved for the Li_2S/CNT/C-N/O, especially at the initial charging stage of polysulfides nucleation, which shed light on the improved reactive kinetics and active material utilization.

1. Introduction

The demand for high-energy-storage system is increasing as the development of electric and smart grid. Thus, much attention has been paid to lithium-chalcogen batteries [1–3]. Among these, lithium-sulfur (Li-S) battery, using sulfur as cathode and lithium as anode, is regarded

---

* Corresponding author.
E-mail address: jbzhao@xmu.edu.cn (J. Zhao).

https://doi.org/10.1016/j.cej.2018.04.049
Received 30 January 2018; Received in revised form 14 March 2018; Accepted 7 April 2018
Available online 07 April 2018

as one of the most promising next-generation high-energy-storage systems as its high theory specific energy (1675 mAh g^{-1}) and high energy (2600 Wh kg^{-1}) [1]. In addition, the elemental sulfur is abundant, low-cost and environmentally friendly. Nevertheless, the commercial application of Li-S batteries is still hindered by some inherent issues, including the poor electronic conductivity of sulfur, the large volume change (~79%) of electrode, and the dissolution and shuttle of medium products polysulfides [4,5].

To solve above problems, the most popular strategy is to bring sulfur into carbon hosts, such as hollow carbon, carbon nanotube (CNT) and graphene [6–8]. A melting diffusing method is normally adopted to bring sulfur into pre-prepared carbon hosts since the low melting point of sulfur (155 °C). However, there is still inevitable sulfur remaining on the outside or diffusing out from the porous structure [7,9]. By contrast, the lithium sulfide (Li_2S), a fully lithiated sulfur product, is proposed as an alternative cathode due to its high theoretical specific energy (1166 mAh g^{-1}) as the sulfur [10]. Most importantly, the high thermal stability of Li_2S (melting point of 1372 °C [11]) makes it available to confine sulfur species under high temperature condition.

Though these appealing advantages, the Li_2S cathode also suffers from its inherent problems. One problem is same with the sulfur cathode — the dissolution and shuttle of polysulfides, leading to fast capacity fading and lithium anode corrosion. A variety of strategies have been proposed to suppress the polysulfides dissolution for sulfur cathode, such as physical confinement, chemical adsorption, inserting interlayers and modified separators [12–18]. Another problem is that Li_2S shows both poor electronical and ionic conductivity. Early attempts are mainly focused on resolving the electron conductivity. For example, various Li_2S/metal or Li_2S/carbon composites are investigated to improve Li_2S utilization [19–21]. Nevertheless, a desirable capacity and cycling stability is still not achieved. A breakthrough is made by Yang et al., who adopted a high cut-off voltage to render Li_2S electrochemical activation [22]. As the poor electron and ion transfer, it is difficult for lithium ion (Li-ion) to extract from Li_2S to form polysulfide phase, leading to a large potential barrier in the first charging process. Thus, an extra energy is needed to overcome this barrier for the nucleation of polysulfides. Therefore, for the Li_2S cathode, it is vital to construct framework with both great electron and ion transportation.

A number of nanostructured composites have been developed as their efficient effect on shortening the distance of ion diffusion on nanoscale [23,24]. For example, Cai et al. prepared nanostructured Li_2S/C composite from commercially micrometer-sized Li_2S through high-energy ball milling [25]. The particle size can be reduced to 200–500 nm, achieving enhanced active material utilization. However, as Li_2S is very sensitive to water and oxygen, harsh synthesized conditions are required. Another alternative precursor, Li_2SO_4, is proposed based on the reaction of $Li_2SO_4 + 2C \rightarrow Li_2S + 2CO_2$ [26,27]. As the fact that Li_2SO_4 is low cost and no complex equipment is needed, fabricating Li_2S from Li_2SO_4 exhibits a promising prospect. However, it is still challenging to fabricate nanostructured Li_2S/C composites using a facile and scale-up synthesis method. In addition, it is vital to get in-depth understanding about the Li-ion transportation in the composite since its important role in the Li_2S cathode.

Herein, the nano-sized Li_2S uniformly embedded in the nitrogen/oxygen dual doped CNT/C conductive network (Li_2S/CNT/C-N/O) composite is fabricated by a simple spray-dried method. Firstly, the spray-dried technology is adopted as its fast and efficient for fabricating the Li_2S/CNT/C-N/O composite on large scale. Secondly, the highly entangled CNT can be connected together with thermal polymerized carbon via a spray-dried process, providing fast electron pathway. Most impressively, hollow structure can be obtained, which can efficiently increase the reaction area between the active material and the electrolyte, providing fast Li-ion diffusion and mass transfer. Furthermore, benefited from the solution reaction, the nanosized Li_2S can be uniformly dispersed in the CNT/C-N/O network, which will guarantee enough electron contact and improve the active material utilization. The electrochemical measurements show that the fabricated Li_2S/CNT/C-N/O cathode exhibits great cycling stability and high rate performance. To explore the fundamental mechanism about the improved performances, the *in-situ* electrochemical impedance spectra (EIS) is carried out to get insightful understanding about the Li-ion diffusion and charge transportation in the composite.

2. Experimental

2.1. Material fabrication

Commercial $Li_2SO_4{\cdot}H_2O$ (Aladdin), carbon nanotube (CNT, Chengdu Institute of Organic Chemistry, Chinese Academy of Sciences), sucrose (Sinopharm Chemical Regent, China) and chitosan (Xilong Chemical Company, China) were used as raw materials without any special treatment. In a typical experiment, $Li_2SO_4{\cdot}H_2O$ (2.0 g), CNT (0.4 g), sucrose (1 g) and chitosan (0.5 g) was added into deionized water (25.0 mL). After stirring at room temperature for 4 h, the mixture was spray-dried with B-290 mini spray dryer (Buchi Company, Switzerland). The setting temperature was 200 °C and pump rate was 6%. Subsequently, the collected precursor was calcined at 500 °C for 30 min, followed by 800 °C for 3 h with 2 °C/min under argon atmosphere. The obtained product is denoted as Li_2S/CNT/C-N/O. The products of Li_2S/CNT/C-N, Li_2S/CNT/C-O, Li_2S/C-N/O and Li_2S/C-N/O were also prepared without adding sucrose, chitosan, CNT, and $Li_2SO_4{\cdot}H_2O$, respectively.

Li_2S_6 solution was synthesized based on previous report [28]: stoichiometric ratio of sulfur and Li_2S was adding into 1,3-dioxolane (DOL), followed by heating at 80 °C with continuously stirring for 12 h. All above procedures were performed in the Ar-filled glovebox.

2.2. Material characterization

The X-ray diffraction (XRD) data were obtained using Rigaku X-ray diffraction with Cu-Kα radiation operated at 40 kV and 15 mA. The morphologies of the composites were characterized using field emission scanning electronic microscope (SEM, HITACHI S-4800) and high-resolution transmission electron microscope (HRTEM, TECNAI F30). The thermal analyzer (SDT-Q600) was utilized to get thermogravimetric analysis (TGA) curves from 30 to 800 °C with the heating rate of 10 °C min^{-1} in air atmosphere. To get the information about Brunauer-Emmett-Teller (BET) specific surface area and pore distribution, the nitrogen adsorption/desorption isotherms were measured with ASAP 2020. Horvath-Kawazoe (HK) and Barrett-Joyner-Halenda (BJH) methodology were used to analyze the micropore and mesopore size distribution, respectively. The X-ray photoelectron spectrum (XPS) was analyzed with Qtac-100 scanning microprobe.

2.3. Cell assembly and electrochemical measurement

The working electrode contained the active material (Li_2S/CNT/C-N/O), acetylene black (AB) and polyvinyl chloride (PVC) with the mass ratio of 80: 10: 10. After stirring thoroughly, the slurry was casted onto Al foil, which was then dried at 60 °C overnight. All the above processes were conducted in an argon-filled glovebox. The electrolyte was 1 M lithium bis(trifluoromethanesulfonyl)imide (LiTFSI) in 1,2-dimethoxyethane (DME) and DOL (DME: DOL = 1: 1, v/v) with 1 wt% $LiNO_3$. The ratio of electrolyte to sulfur is 10 mL·g^{-1}. The lithium metal foil was used as both counter and reference electrode. By contrast, commercial Li_2S was used as cathode, with Li_2S/AB/PVC ratio of 50: 40: 10. A typical Li_2S mass loading is ~2 mg·cm^{-2}. The cyclic voltammetry (CV) profiles were measured at a scanning rate of 0.05 mV s^{-1} with a voltage range 1.75–2.8 V after initial activating to 3.4 V. The discharge and charge plots were collected using battery system (LAND CT2001A instrument).

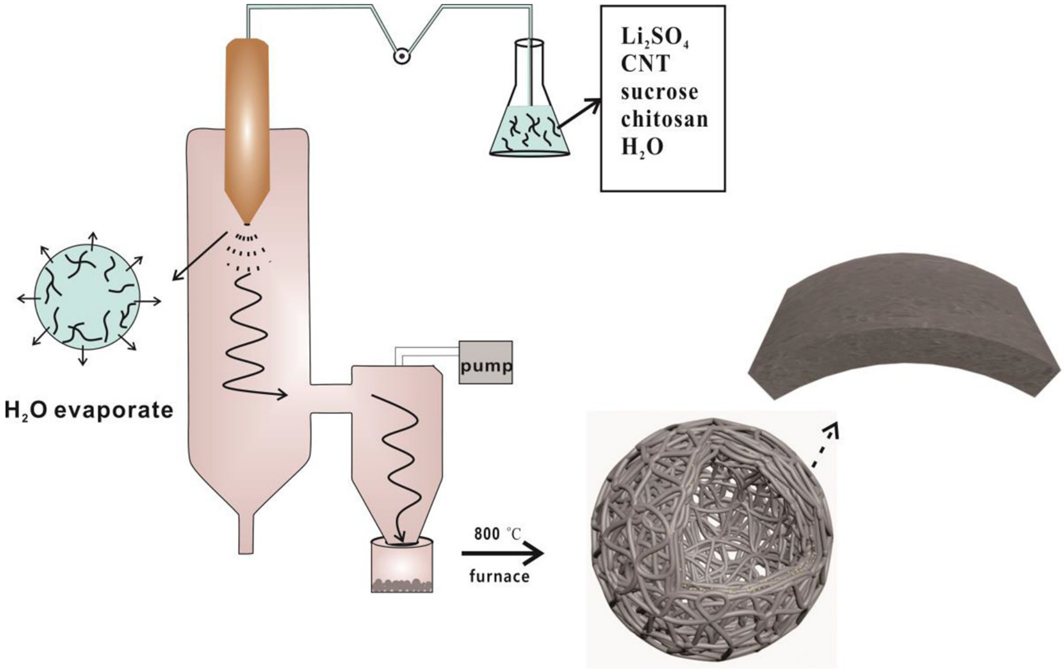

Fig. 1. The schematic process of Li_2S/CNT/C-N/O preparation.

2.4. In-situ electrochemical impedance spectra test

(EIS) were carried on Autolab using two-electrode system with lithium metal as both counter and reference electrode. The charge/discharge process was tested at 30 mA g^{-1} between 1.75 and 3.4 V. The Nyquit points were collected after resting for 10 min. The applied amplitude was 5 mV with frequency range of 0.1 Hz - 100 kHz.

3. Results and discussion

The schematic process of Li_2S/CNT/C-N/O fabrication is illustrated in the Fig. 1. Herein, the Li_2SO_4 is adopted as Li_2S precursor, the CNT is chosen as the electron conductive skeleton, the sucrose acts as reactive carbon precursor, coating reagent on Li_2S as well as O-dopant, and the chitosan is utilized to produce N-dopant. The fabrication of Li_2S/CNT/C-N/O mainly contains two steps. Firstly, the raw reagents are fed into a spray dryer via a peristaltic pump. The water can be rapidly evaporated under high temperature, yielding remained solid of Li_2SO_4/CNT/sucrose/chitosan assembled together in a three dimensional (3D) spherical structure (Fig. S1). After subsequent annealing at 800 °C for 3 h, the product of Li_2S/CNT/C-N/O can be synthesized via a typical reaction: $Li_2SO_4 + 2C \rightarrow Li_2S + 2CO_2$. As a result, the composite composed of nano-sized Li_2S and CNT/C-N/O framework is obtained with enough amount of carbon.

To confirm the successful fabrication of Li_2S, the XRD data of as-prepared composites are collected, as shown in the Fig. 2a. For pristine CNT, two typical carbon material peaks can be detected. The strong peak at 26.6° belongs to the (0 0 4) of carbon and the weak peak at 44.6° is attributed to the (1 0 2). As for obtained Li_2S/CNT/C-N/O, the reflections can be well match with the crystalline data of Li_2S (JCPDS card 065–2981) except the peaks from the CNT and the Kapton tape (Fig. S2a) used to protect Li_2S. The peaks at 26.98°, 31.28°, 44.80°, 53.08°, 65.20° and 71.97° correspond to the (1 1 1), (2 0 0), (2 2 0), (3 1 1), (4 0 0) and (3 3 1) planes of Li_2S, respectively. The same reflections are found in the commercial Li_2S (Fig. S2b). No other impurities are detected in the obtained Li_2S/CNT/C-N/O composite, indicating the complete reaction of Li_2SO_4 (Fig. S2c) to Li_2S. The XRD results demonstrate the successful fabrication of Li_2S from the raw material of Li_2SO_4. Both SEM and TEM images are used to characterize the morphologies of commercial Li_2S and as-prepared Li_2S/CNT/C-N/O composite. Commercial Li_2S sample shows micro-size from 1 to 10 μm, mainly concentrated at 3–6 μm (Fig. S3a). From Fig. 2b, it can be seen that the Li_2S/CNT/C-N/O composite is spherical morphology with size range from few hundreds nm to ~30 μm (insert in Fig. 2b). After strongly mechanical grinding, the hollow structure can be identified in either small size (Fig. S3b) or large size (Fig. S3c), which can increase the contacted area between electrolyte and active material. The enlarged SEM image (Fig. 2c) displays that the CNT and carbon material are interconnected with some pore structures, which is beneficial for Li-ion diffusion. If without the introduction of CNT, agglomerated microparticles are obtained (Fig. S3d), indicating the important role of CNT in constructing spherical morphology. Further character is performed using TEM image (Fig. 2d). As we can see from high-resolution TEM (HR-TEM) images, two different lattice stripes are identified (Fig. S4), which are more obvious in the Fourier Transformed image (inserted Fig. 2e). The distance of 0.33 nm belongs to the (1 1 1) plane of Li_2S, the size of which is around 5 nm. The distance of 0.35 nm is attributed to the (0 0 4) of CNT, and outside amorphous carbon shell comes from the carbonized sucrose and chitosan. The results are well agreed with the XRD analysis. Further TEM-mapping images (Fig. 2f–j) demonstrate the uniform distribution of C, N, O and S elements in the Li_2S/CNT/C-N/O. From the above characterization of morphologies, it can be seen that the nano-sized Li_2S particles are well confined in the CNT/C-N/O framework.

The amount of Li_2S in the composite is determined from the TGA result (Fig. 3a). According to the reaction between Li_2S and carbon materials in air atmosphere, the final product should be Li_2SO_4 [27,29]. Figure S5 also verifies that there is no weight remained for pure CNT calcined to 800 °C in air atmosphere. Therefore, the mass percentage of Li_2S in Li_2S/CNT/C-N/O is calculated to be 60.2%. According to theeelement analysis, the percentage of C and N is 33% and 2%, respectively. Thus, the percentage of O is calculated to be 4.8%. Nitrogen adsorption and desorption isotherms are measured to analyzed the porous information of Li_2S/CNT/C-N. As shown in Fig. 3b, the nitrogen isothermal curves indicate mesoporous structure feature in Li_2S/CNT/C-N/O composite. The pore size distribution states the coexistence of microporous, mesoporous and macroporous structures (Fig. 3c, Fig. S6). The microporous is concentrated at ~0.8 nm from HK methodology,

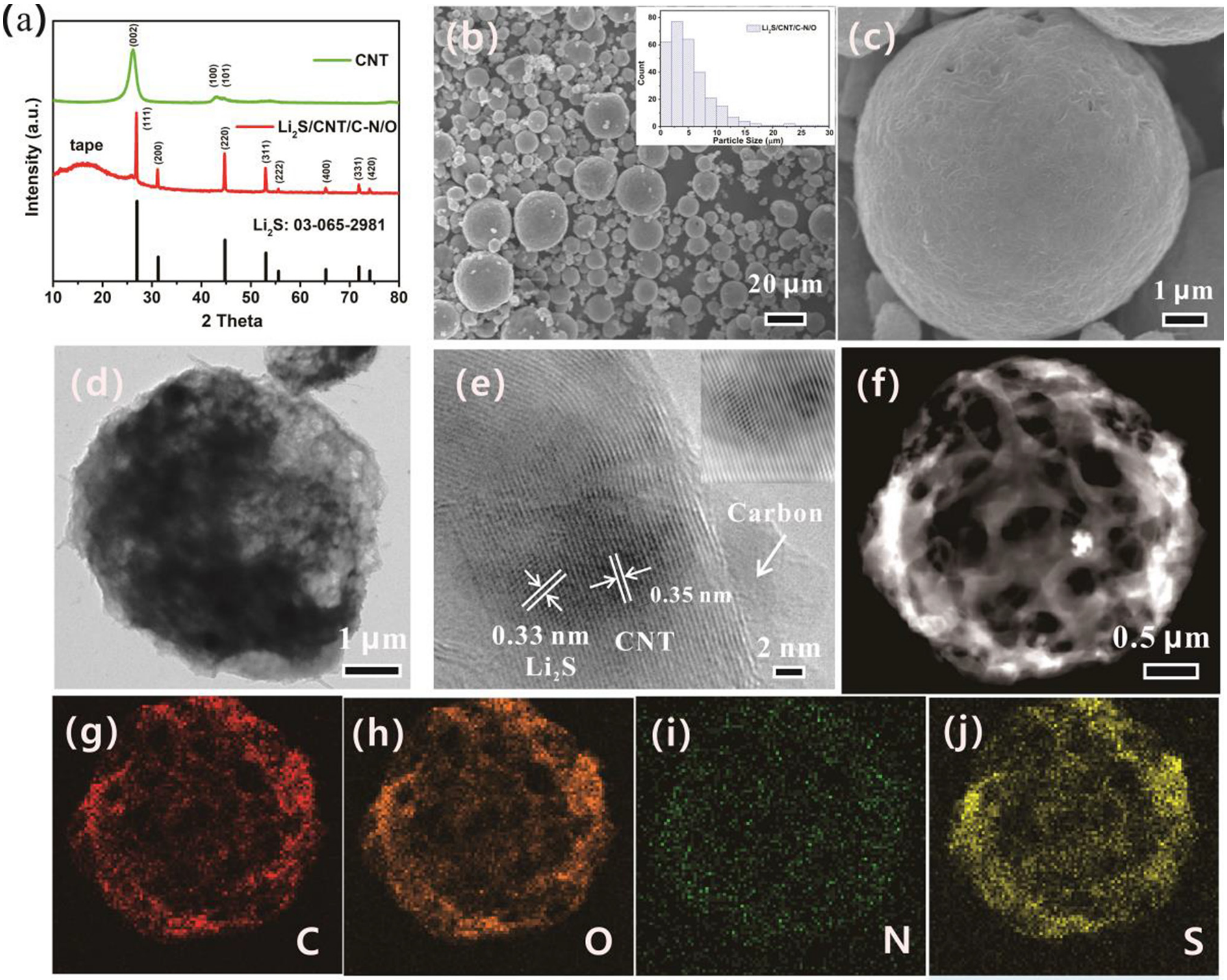

Fig. 2. (a) The XRD spectra, (b, c) SEM images of Li_2S/CNT/C-N/O (inserted Fig. 2b, the statistics of Li_2S/CNT/C-N/O particle size distribution obtained from image-pro plus 6.0 software), (d) TEM and (e) HR-TEM images of Li_2S/CNT/C-N/O, (f) STEM images of Li_2S/CNT/C-N/O and (g - j) corresponding elemental mapping of (g) C, (h) O, (i) N, (j) S.

while mesopore is mainly distributed at ~4 nm, which is beneficial for physically adsorbing polysulfides.[30] Besides, there is a broad macroporous distribution from ~10 to ~60 nm originated from the cross-linking of highly entangled CNT, facilitating electrolyte infiltration. The Brunauer-Emmett-Teller (BET) specific area of Li_2S/CNT/C-N/O is measured to be 53.4 $m^2\ g^{-1}$. These results are well agreed with the SEM and TEM characterization, confirming the existence of porous structure in the Li_2S/CNT/C-N/O composite.

The XPS spectra are used to analyze the chemical environment of as-prepared composite. Fig. 3d displays the survey spectrum of Li_2S/CNT/C-N/O. The emergence of N and O signals estimates the co-existence of N and O dopants. Carefully dividing the C 1 s spectrum (Fig. 3e), four peaks attributed to the interaction of C—C/C═C, C—O, C—N—C and COOH can be obtained,[31] confirming the N/O doped into CNT/C skeleton. It is believed that the N and O dopants in carbon can facilitate strong adsorption interaction for polysulfides.[6,32] To investigate the interaction of Li_2S in the composite, the Li 1 s and S 2p XPS spectra of pure Li_2S and Li_2S/CNT/C-N/O are compared (Fig. 3f, Fig. S7). As shown in Fig. S7, the S 2p peaks in Li_2S/CNT/C-N/O composite shift to higher energy than that of pure Li_2S, indicating a decrease in electron density.[33] This could be attributed to the interaction of Li-N in Li_2S/CNT/C-N/O. From further Li 1 s XPS spectra (Fig. 3f), we can see that apart from the same peak at 54.6 eV (Li-S), additional peak at 55.5 eV can be identified in Li_2S/CNT/C-N/O, confirming the Li-N interaction between Li_2S and CNT/C-N/O framework [34,35].

To evaluate the electrochemical performances, the obtained Li_2S/CNT/C-N/O composite is assembled as cathode to compare with the pristine Li_2S cathode. As an initial barrier exists in Li_2S, a high cut-off voltage is common adopted to overcome potential barrier [22]. Herein, the initial cycle is swept from open voltage ~2.5 to 3.4 V (vs. Li/Li^+) to make Li_2S electrochemically active. Fig. 4a, b shows the typical CV curves of Li_2S/CNT/C-N/O and Li_2S cathode in the initial five cycles. In the first cathodic scanning, an initial peak started from 2.6 V is observed for the Li_2S/CNT/C-N/O, which corresponds to the nucleation of polysulfides from Li_2S [22]. By contrast, a higher overpotential is found in Li_2S (~2.9 V), suggesting that higher energy is needed to overcome the potential barrier due to its large particle [29]. The lower active potential of Li_2S/CNT/C-N/O can be attributed to the small size of Li_2S, providing shorter pathway for Li-ion to extract from Li_2S. After initial activation, the following cycles are scanned between 1.75 and 2.8 V. The obtained CV curves are quite similar with that of traditional sulfur cathode. During the cathodic scanning, there are two main reduction peaks. The first peak at ~2.3 V reflects the reduction from sulfur to long-chain lithium polysulfides (Li_2S_x, $4 \le x \le 8$), while the second peak at ~2.02 V belongs to the further formation of Li_2S_2/Li_2S. Notably, additional peak at ~2.14 V appears in the first cycle, which is caused by the poorly stable intermediate species produced [25,36]. For the anodic scanning, two main peaks at ~2.30 and 2.40 V are observed,

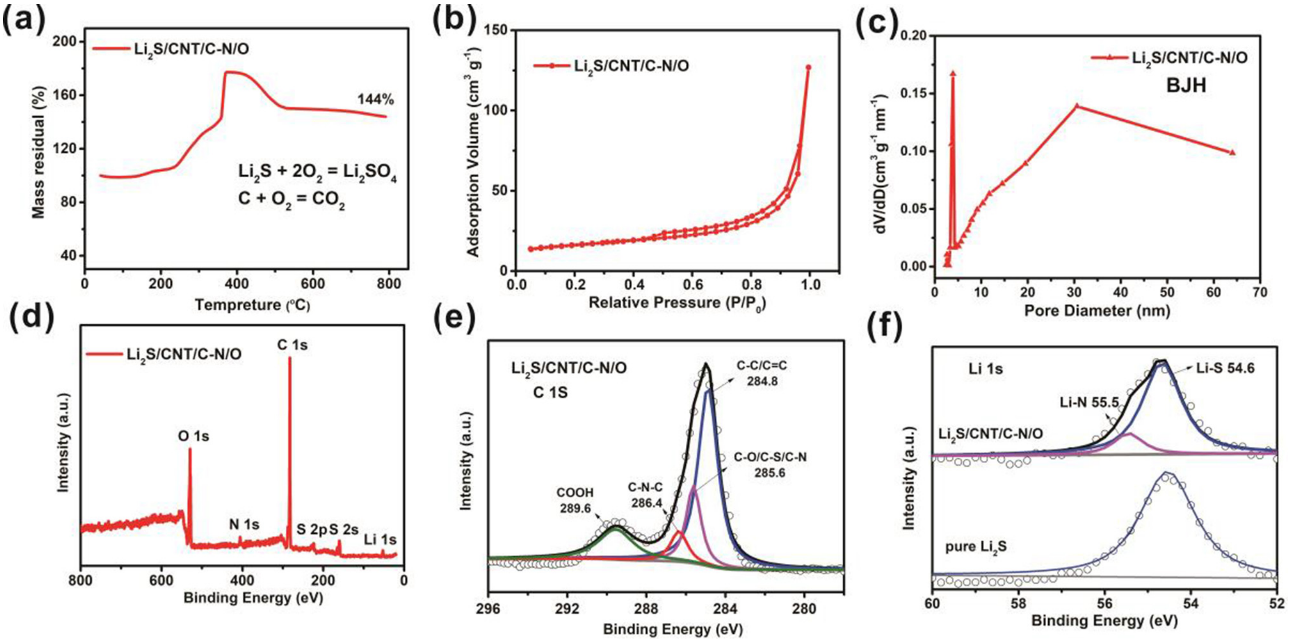

Fig. 3. (a) TGA curves of Li_2S/CNT/C-N/O in air, (b) Nitrogen adsorption-desorption isotherms of Li_2S/CNT/C-N/O, (c) corresponding mesoporous size distribution based on BJH methodology, (d) survey XPS spectrum of Li_2S/CNT/C-N/O, (e) C 1 s XPS spectrum of Li_2S/CNT/C-N/O, (f) Li 1 s XPS spectra of Li_2S/CNT/C-N/O and Li_2S.

reflecting the transformation from Li_2S_2/Li_2S to polysulfides [37]. The well overlapped curves during the following four cycles suggest the great electrochemical reactive stability.

The corresponding charge/discharge profiles are obtained at 200 mA g^{-1} after initial activation at 30 mA g^{-1}. As shown in Fig. 4c and d, both cathodes present a typical charging barrier in the initial stage, which is associated with the nucleation of polysulfides [22]. The barrier heights of pristine Li_2S and Li_2S/CNT/C-N/O cathodes are 0.67 and 0.08 V, respectively. The smaller amplitude for the Li_2S/CNT/C-N/O cathode indicates that lower energy is required to extract Li-ion from bulk Li_2S. This observation is in good consistent with the results from CV, suggesting improved Li-ion transportation for nano-sized Li_2S in CNT/C-N/O framework. In the subsequent discharging process, two typical discharging plateaus are observed, similar to the common sulfur cathode. The first discharged capacity of Li_2S/CNT/C-N/O can reach up to 1014 mAh g^{-1}, which is much higher than that of pure Li_2S (696 mAh g^{-1}). The dramatic increase in capacity for Li_2S/CNT/C-N/O can be ascribed to the great electron conductivity and polysulfides affinity, facilitating the utilization of active material Li_2S. The cycling performances of the prepared Li_2S/CNT/C-N/O and pristine Li_2S cathodes are compared at 200 mA g^{-1}. As shown in Fig. 4e, the pristine Li_2S cathode exhibits low coulombic efficiency and fast capacity decay, remaining only 350 mAh g^{-1} after 200 cycles. By contrast, a high coulombic efficiency and stable cycling behavior is achieved in Li_2S/CNT/C-N/O. A reversible discharge capacity is stabilized at 671 mAh g^{-1} with capacity decay of 0.03% per cycle after 200 cycles. In addition, Li_2S/CNT/C-N/O cathode exhibits higher capacity and stability than that of Li_2S/CNT/C-N and Li_2S/CNT/C-O (Fig. S8a), demonstrating the efficiently N/O dual-doping in improving electrochemical performances. Most impressively, the great capacity stability at high current density is also achieved for Li_2S/CNT/C-N/O cathode (Fig. 4f.). For the pristine Li_2S cathode, there is a fast capacity fading at high rates. When the current density is applied to 1000 mA g^{-1}, only capacity of ~100 mAh g^{-1} is released for the Li_2S cathode. By contrast, the Li_2S/CNT/C-N/O cathode exhibits higher capacity retention of 714, 577, 456, and 390 mAh g^{-1} at current density of 500, 1000, 2000, 3000 mA g^{-1}, respectively. When the current rate returns back to 200 mA g^{-1}, the capacity of 747 mAh g^{-1} can be still well remained. Even at high current rates, the charge/discharge curves of Li_2S/CNT/C-N/O cathode are still identical (Fig. S8b–c). For practical application, Li_2S/CNT/C-N/O cathode with high loading mass of 3.5 mg · cm^{-2} is also evaluated. Still, a stable cycling performance can be obtained (Fig. S8d) at 500 mA g^{-1}. Compares with recent work (Table S1), Li_2S/CNT/C-N/O cathode in this work exhibit considerable capacity and cyclability. Above results reveal that the Li_2S/CNT/C-N/O cathode exhibits significant improvements in rate and cycling stability, indicating good electron and Li-ion transportation as well as polysulfides adsorption property.

To confirm the strong affinity of CNT/C-N/O to polysulfides, the polysulfide adsorption experiment was conducted to give visual observation. Taken Li_2S_6 as a representative, the result is exhibited in Fig. S9. The tawny color of Li_2S_6 solution changes to completely colorless after adding CNT/C-N/O, indicating strong adsorption of Li_2S_6 by CNT/C-N/O. Besides, to get more information about the cycled cathodes, the surface morphologies of the Li_2S/CNT/C-N/O and Li_2S electrodes are detected before and after 100 cycles. As shown in the Fig. S10, the pristine Li_2S cathode suffers from serious agglomeration after 100 cycles. Such agglomeration is caused by the reduplicative dissolution/deposition of polysulfides, which will impact the diffusion and transportation of Li-ion [38,39]. In comparison, little change is found in the Li_2S/CNT/C-N/O electrode. Even after 100 cycles, the structure of spherical morphology can be still clearly observed. The well rigid 3D structure of CNT/C-N/O can continuously provide great electron and ion transfer for active material Li_2S, maintaining efficient intergranular contact.

For better understanding the electrochemical reaction kinetics in Li_2S/CNT/C-N/O cathode, *in-situ* EIS study is conducted to study the initial charge/discharge process. Fig. 5a shows the initial charge/discharge curves of Li_2S/CNT/C-N/O cathode and corresponding tested points during the *in-situ* EIS. The obtained Nyquist plots of Li_2S/CNT/C-N/O and Li_2S cathode during the charge and discharge process are displayed in Fig. 5b and Fig. S11, respectively. The equivalent circuit of EIS spectrum is displayed in Fig. S11e. Corresponding electrochemical reaction during the charging is also illustrated below the Fig. S11. The fitting result suggests that Nyquist plots consist of two semicircles. The semicircle in high-frequency can be interpreted as the whole surface

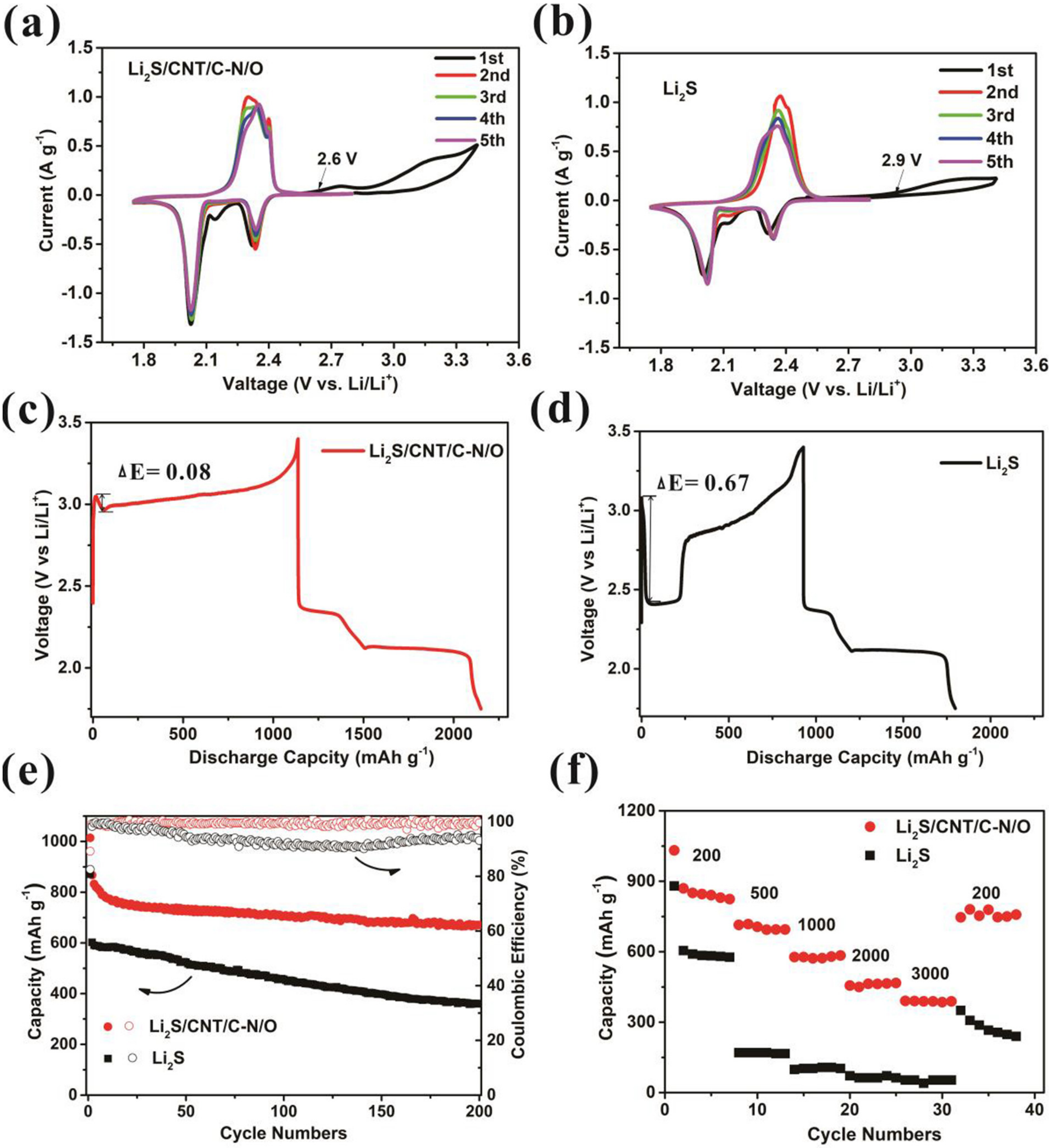

Fig. 4. CV curves of (a) Li_2S/CNT/C-N/O (b) Li_2S at scanning rate of $0.05\,mV\,s^{-1}$, (c, d) initial discharge/charge profiles of (c) Li_2S/CNT/C-N/O (d) Li_2S at $30\,mA\,g^{-1}$, (e) cycling performances of Li_2S/CNT/C-N/O and Li_2S at $200\,mA\,g^{-1}$, (f) rate performances of Li_2S/CNT/C-N/O and Li_2S at the current density of 200, 500, 1000, 2000, and $3000\,mA\,g^{-1}$.

impedance (R_s) of both electrodes, including cathode and lithium anode [40]. The semicircle in middle-frequency can be used to describe the resistance of charge transfer (R_{ct}) on the cathode. One inclined line at low frequency region represents the Warburg impedance (W_o), which is related with the Li-ion diffusion in bulk Li_2S. R_e stands for the electrolyte resistance. The specific simulated values of Li_2S/CNT/C-N/O and Li_2S cathode at different states of charge (DOC) and discharge (DOD) are compared in Fig. 5c. For the pristine Li_2S cathode, there is a gradual growing for R_e during the first charge process. The increased R_e can be attributed to the increased viscosity of electrolyte, which is triggered by the polysulfides dissolution [40]. By contrast, the value of R_e is relatively stable for the Li_2S/CNT/C-N/O. In the subsequent discharging, the R_e for Li_2S/CNT/C-N/O is still lower than that of Li_2S, indicating less polysulfides diffusion into electrolyte. This could be attributed to the physical confinement and chemical adsorption in the CNT/C-N/O framework, efficiently anchoring polysulfides on the cathode. As for the comparison of R_s and R_{ct}, it can be clearly seen an obvious gap, especially at period of 0.1% ~ 5% DOC and 80% DOD. The stage of 0.1%~5% DOC corresponds to the nucleation of polysulfides, and ~80% DOD can be assigned to the formation of Li_2S_2/Li_2S during the discharging process. A large R_{ct} resistance is found in Li_2S (~1000 and ~2000 Ohm, respectively), owning to the difficult electron and ion transportation in large particle size of Li_2S. Notably, a dramatic reduced R_{ct} is obtained for the Li_2S/CNT/C-N/O (~30 and 450 Ohm). Furthermore, even during the whole charge/discharge process, the Li_2S/CNT/C-N/O cathode still shows smaller R_s and R_{ct}

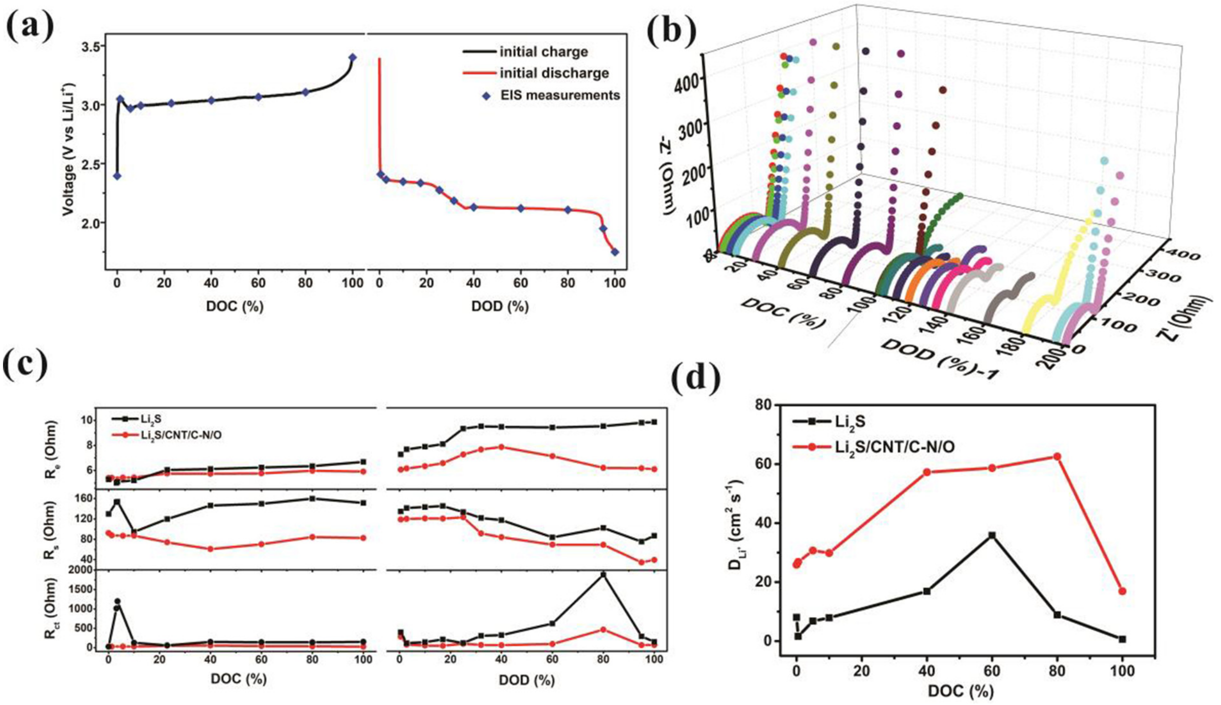

Fig. 5. (a) initial charge/discharge curves of Li_2S/CNT-/C-N/O and EIS measured points, (b) Nyquist plots in *in-situ* EIS, (c) the comparison of R_e, R_s and R_{ct} between Li_2S and Li_2S/CNT-/C-N/O, (d) diffusion coefficient of Li-ion ($D_{Li}{}^+$) from EIS.

than that of Li_2S, suggesting fast Li-ion and charge transfer.

To further compare the Li-ion diffusion in the Li_2S/CNT/C-N/O and pristine Li_2S, the diffusion coefficient of Li-ion ($D_{Li}{}^+$) is quantified from the inclined line in the Warburg region [41]. Specific calculation process is described in the Supporting Information (Fig. S12). As shown in Fig. 5d, the $D_{Li}{}^+$ of Li_2S is only $1.61 \times 10^{-18}\,cm^2\,s^{-1}$ at the point of 0.1% DOC, corresponding to the nucleation of polysulfides. By contrast, about an order of magnitude higher value ($2.68 \times 10^{-17}\,cm^2\,s^{-1}$) is found for the Li_2S/CNT/C-N/O cathode. It is well explained that low energy is needed for Li-ion extraction from Li_2S/CNT/C-N/O (Fig. 4a–d). With the aging of charging process, an increasing tendency of $D_{Li}{}^+$ is observed for both cathodes, owing to the formation of liquid phase polysulfides. At the end charging stage, there is a drop in $D_{Li}{}^+$ caused by the formation of Li_2S_8 or S_8 [22,42]. During the whole initial charging, a still higher $D_{Li}{}^+$ is exhibited for the Li_2S/CNT/C-N/O than Li_2S. Besides, the $D_{Li}{}^+$ is also calculated based on different rate CV (Supporting Information and Fig. S13) [43,44]. A higher value is obtained for Li_2S/CNT/C-N/O than that of Li_2S, confirming that the fabricated CNT/C-N/O framework can provide great transport for Li-ion. Above discussions demonstrate the advanced structure design of Li_2S/CNT/C-N/O. Nanosized Li_2S can efficiently reduce the distance of Li-ion to active material, facilitating active material utilization. In addition, the CNT/C-N/O conductivity network provide fast conductivity of electron, dramatically improving the electrochemically reactive kinetics.

4. Conclusion

In conclusion, a spray-dried method is used to prepare the Li_2S/CNT/C-N/O composite, in which the nanosized Li_2S is uniformly distributed in the CNT/C-N/O host. The constructed CNT/C-N/O skeleton can provide fast electron pathway and great ion diffusion channel. The N/O dopants can effectively reduce the active material loss. As a result, the Li_2S/CNT/C-N/O cathode delivers high initial discharge capacity of $1014\,mAh\,g^{-1}$, remaining $671\,mAh\,g^{-1}$ with capacity decay of 0.03% per cycle after 200 cycles at current density of $200\,mA\,g^{-1}$. Even at higher current rate of 500, 1000, 2000 and $3000\,mA\,g^{-1}$, a stable capacity can be still achieved for the Li_2S/CNT/C-N/O. The in-depth understanding about the great electrochemical behavior of the Li_2S/CNT/C-N/O is studied by *in-situ* EIS. The smaller R_s and R_{ct} and higher $D_{Li}{}^+$ are found for the Li_2S/CNT/C-N/O than the pristine Li_2S cathode, especially at the charging stage of polysulfides nucleation, which contribute significant improvements to the electrochemical reaction kinetics and active material utilization. We believe that the same strategy can be adopted to fabricate nanostructured carbon-based composite, opening a promising platform for constructing both electron and ion conductivity framework.

Acknowledgement

This work is supported by the National Natural Science Foundation of China (Grant No. 2127318 and No.21621091) and National Found for Fostering Talents of Basic Science (J1310024). The authors also wish to express their thanks to Prof. Daiwei Liao for his valuable suggestion.

Appendix A. Supplementary data

Supplementary data associated with this article can be found, in the online version, at http://dx.doi.org/10.1016/j.cej.2018.04.049.

References

[1] Z.W. Seh, Y. Sun, Q. Zhang, Y. Cui, Designing High-Energy Lithium-Sulfur Batteries, Chem. Soc. Rev. 5605–5634 (2016).

[2] J. He, Y. Chen, W. Lv, K. Wen, P. Li, Z. Wang, W. Zhang, W. Qin, W. He, Three-Dimensional Hierarchical Graphene-CNT@Se: A Highly Efficient Freestanding Cathode for Li–Se Batteries, ACS Energy Lett. 1 (2016) 16–20.

[3] J. He, Y. Chen, W. Lv, K. Wen, Z. Wang, W. Zhang, Y. Li, W. Qin, W. He, Three-Dimensional Hierarchical Reduced Graphene Oxide/Tellurium Nanowires: A High-Performance Freestanding Cathode for Li-Te Batteries, ACS Nano 10 (2016) 8837–8842.

[4] X. Ji, L.F. Nazar, Advances in Li–S batteries, J. Mater. Chem. 20 (2010) 9821–9826.

[5] S.S. Zhang, Liquid electrolyte lithium/sulfur battery: Fundamental chemistry, problems, and solutions, J. Power Sources 231 (2013) 153–162.

[6] Y. Peng, Y. Zhang, J. Huang, Y. Wang, H. Li, B.J. Hwang, J. Zhao, Nitrogen and oxygen dual-doped hollow carbon nanospheres derived from catechol/polyamine as

sulfur hosts for advanced lithium sulfur batteries, Carbon 124 (2017) 23–33.

[7] D. Gueon, J.T. Hwang, S.B. Yang, E. Cho, K. Sohn, D.K. Yang, J.H. Moon, Spherical Macroporous Carbon Nanotube Particles with Ultrahigh Sulfur Loading for Lithium-Sulfur Battery Cathodes, ACS Nano 12 (2018) 226–233.

[8] Y. Zhang, K. Li, J. Huang, Y. Wang, Y. Peng, H. Li, J. Wang, J. Zhao, Preparation of Monodispersed Sulfur Nanoparticles-Partly Reduced Graphene Oxide-Polydopamine Composite for Superior Performance Lithium-Sulfur Battery, Carbon 114 (2017) 8–14.

[9] L. Borchardt, M. Oschatz, S. Kaskel, Carbon Materials for Lithium Sulfur Batteries-Ten Critical Questions, Chemistry 22 (2016) 7324–7351.

[10] Y. Son, J.-S. Lee, Y. Son, J.-H. Jang, J. Cho, Recent Advances in Lithium Sulfide Cathode Materials and Their Use in Lithium Sulfur Batteries, Adv. Energy Mater. 5 (2015).

[11] P.T. Cunningham, S.A. Johnson, C.E. J, Phase Equilibria in Lithium-Chalcogen Systems II. Lithium-Sulfur, J. Electrochem. Soc. 119 (1972) 1448–1450.

[12] J. He, Y. Chen, W. Lv, K. Wen, C. Xu, W. Zhang, W. Qin, W. He, Three-Dimensional CNT/Graphene–Li2S Aerogel as Freestanding Cathode for High-Performance Li–S Batteries, ACS Energy Lett. 1 (2016) 820–826.

[13] X. Li, M. Gao, W. Du, B. Ni, Y. Wu, Y. Liu, C. Shang, Z. Guo, H. Pan, A mechanochemical synthesis of submicron-sized Li2S and a mesoporous Li2S/C hybrid for high performance lithium/sulfur battery cathodes, J. Mater. Chem. A 5 (2017) 6471–6482.

[14] Y. Wu, T. Momma, S. Ahn, T. Yokoshima, H. Nara, T. Osaka, On-site chemical prelithiation of S cathode at room temperature on a 3D nano-structured current collector, J. Power Sources 366 (2017) 65–71.

[15] L. Qie, A. Manthiram, Uniform Li2S precipitation on N, O-codoped porous hollow carbon fibers for high-energy-density lithium-sulfur batteries with superior stability, Chem. Commun. (Camb.) 52 (2016) 10964–10967.

[16] Y. Hwa, J. Zhao, E.J. Cairns, Lithium Sulfide (Li2S)/Graphene Oxide Nanospheres with Conformal Carbon Coating as a High-Rate, Long-Life Cathode for Li/S Cells, Nano Lett. 15 (2015) 3479–3486.

[17] L. Qie, A. Manthiram, High-Energy-Density Lithium-Sulfur Batteries Based on Blade-Cast Pure Sulfur Electrodes, ACS Energy Lett. 1 (2016) 46–51.

[18] S.-H. Chung, C.-H. Chang, A. Manthiram, Hierarchical sulfur electrodes as a testing platform for understanding the high-loading capability of Li-S batteries, J. Power Sources 334 (2016) 179–190.

[19] M.N. Obrovac, J.R. Dahn, Electrochemically Active Lithia/Metal and Lithium Sulfide/Metal Composites, Electrochem. Solid-State Lett. 5 (2002) 70–73.

[20] A. Hayashi, R. Ohtsubo, M. Tatsumisago, Electrochemical performance of all-solid-state lithium batteries with mechanochemically activated Li2S–Cu composite electrodes, Solid State Ionics 179 (2008) 1702–1705.

[21] T. Takeuchi, H. Sakaebe, H. Kageyama, H. Senoh, T. Sakai, K. Tatsumi, Preparation of electrochemically active lithium sulfide–carbon composites using spark-plasma-sintering process, J. Power Sources 195 (2010) 2928–2934.

[22] Y. Yang, G. Zheng, S. Misra, J. Nelson, M.F. Toney, Y. Cui, High-capacity micrometer-sized Li2S particles as cathode materials for advanced rechargeable lithium-ion batteries, J. Am. Chem. Soc. 134 (2012) 15387–15394.

[23] J. Cao, C. Chen, Q. Zhao, N. Zhang, Q. Lu, X. Wang, Z. Niu, J. Chen, A Flexible Nanostructured Paper of a Reduced Graphene Oxide-Sulfur Composite for High-Performance Lithium-Sulfur Batteries with Unconventional Configurations, Adv. Mater. 28 (2016) 9629–9636.

[24] C. Nan, Z. Lin, H. Liao, M.K. Song, Y. Li, E.J. Cairns, Durable carbon-coated Li2(S) core-shell spheres for high performance lithium/sulfur cells, J. Am. Chem. Soc. 136 (2014) 4659–4663.

[25] K. Cai, M.K. Song, E.J. Cairns, Y. Zhang, Nanostructured Li(2)S-C composites as cathode material for high-energy lithium/sulfur batteries, Nano Lett. 12 (2012) 6474–6479.

[26] M. Kohl, J. Brückner, I. Bauer, H. Althues, S. Kaskel, Synthesis of highly electrochemically active Li2S nanoparticles for lithium–sulfur-batteries, J. Mater. Chem. A 3 (2015) 16307–16312.

[27] J. Liu, H. Nara, T. Yokoshima, T. Momma, T. Osaka, Micro-scale Li 2 S-C composite preparation from Li 2 SO 4 for cathode of lithium ion battery, Electrochim. Acta 183 (2015) 70–77.

[28] S.S. Zhang, J.A. Read, A new direction for the performance improvement of rechargeable lithium/sulfur batteries, J. Power Sources 200 (2012) 77–82.

[29] D.H. Wang, X.H. Xia, D. Xie, X.Q. Niu, X. Ge, C.D. Gu, X.L. Wang, J.P. Tu, Rational in-situ construction of three-dimensional reduced graphene oxide supported Li2S/C composite as enhanced cathode for rechargeable lithium–sulfur batteries, J. Power Sources 299 (2015) 293–300.

[30] N. Jayaprakash, J. Shen, S.S. Moganty, A. Corona, L.A. Archer, Porous Hollow Carbon@Sulfur Composites for High-Power Lithium-Sulfur Batteries, Angew. Chem. Int. Ed. 50 (2011) 5904–5908.

[31] J. Zhang, Y. Shi, Y. Ding, L. Peng, W. Zhang, G. Yu, A Conductive Molecular Framework Derived Li2S/N, P-Codoped Carbon Cathode for Advanced Lithium-Sulfur Batteries, Adv. Energy Mater. 7 (2017).

[32] T.Z. Hou, X. Chen, H.J. Peng, J.Q. Huang, B.Q. Li, Q. Zhang, B. Li, Design Principles for Heteroatom-Doped Nanocarbon to Achieve Strong Anchoring of Polysulfides for Lithium-Sulfur Batteries, Small 12 (2016) 3283–3291.

[33] Q. Pang, J. Tang, H. Huang, X. Liang, C. Hart, K.C. Tam, L.F. Nazar, A nitrogen and sulfur dual-doped carbon derived from polyrhodanine@cellulose for advanced lithium-sulfur batteries, Adv. Mater 27 (2015) 6021–6028.

[34] Z.W. Seh, H. Wang, N. Liu, G. Zheng, W. Li, H. Yao, Y. Cui, High-capacity Li2S–graphene oxide composite cathodes with stable cycling performance, Chem. Sci. 5 (2014) 1396–1400.

[35] Z.W. Seh, H. Wang, P.-C. Hsu, Q. Zhang, W. Li, G. Zheng, H. Yao, Y. Cui, Facile synthesis of Li2S–polypyrrole composite structures for high-performance Li2S cathodes, Energy Environ. Sci. 7 (2014) 672–676.

[36] C. Barchasz, F. Molton, C. Duboc, J.C. Lepretre, S. Patoux, F. Alloin, Lithium/sulfur cell discharge mechanism: an original approach for intermediate species identification, Anal. Chem. 84 (2012) 3973–3980.

[37] C. Zu, M. Klein, A. Manthiram, Activated Li2S as a High-Performance Cathode for Rechargeable Lithium-Sulfur Batteries, J. Phys. Chem. Lett. 5 (2014) 3986–3991.

[38] S.-E. Cheon, K.-S. Ko, J.-H. Cho, S.-W. Kim, E.-Y. Chin, H.-T. Kim, Rechargeable Lithium Sulfur Battery, J. Electrochem. Soc. 150 (2003) 796–799.

[39] Y. Peng, B. Li, Y. Wang, X. He, J. Huang, J. Zhao, Prussian Blue: A Potential Material to Improve the Electrochemical Performance of Lithium-Sulfur Batteries, ACS Appl. Mater. Inter. 9 (2017) 4397–4403.

[40] V.S. Kolosnitsyn, E.V. Kuzmina, E.V. Karaseva, S.E. Mochalov, A study of the electrochemical processes in lithium–sulphur cells by impedance spectroscopy, J. Power Sources 196 (2011) 1478–1482.

[41] X.-B. Cheng, C. Yan, J.-Q. Huang, P. Li, L. Zhu, L. Zhao, Y. Zhang, W. Zhu, S.-T. Yang, Q. Zhang, The gap between long lifespan Li-S coin and pouch cells: The importance of lithium metal anode protection, Energy Storage Mater. 6 (2017) 18–25.

[42] J. Nelson, S. Misra, Y. Yang, A. Jackson, Y. Liu, H. Wang, H. Dai, J.C. Andrews, Y. Cui, M.F. Toney, In Operando X-ray diffraction and transmission X-ray microscopy of lithium sulfur batteries, J. Am. Chem. Soc. 134 (2012) 6337–6343.

[43] H. Li, Y. Wang, J. Huang, Y. Zhang, J. Zhao, Microwave-assisted Synthesis of CuS/Graphene Composite for Enhanced Lithium Storage Properties, Electrochim. Acta 225 (2017) 443–451.

[44] Y. You, H.R. Yao, S. Xin, Y.X. Yin, T.T. Zuo, C.P. Yang, Y.G. Guo, Y. Cui, L.J. Wan, J.B. Goodenough, Subzero-Temperature Cathode for a Sodium-Ion Battery, Adv. Mater. 28 (2016) 7243–7248.